Nanoscale

Chloride Enables the Growth of Ag Nanocubes and Nanowires by Making PVP Binding Facet-Selective

Journal:	*Nanoscale*
Manuscript ID	NR-ART-12-2022-006762.R1
Article Type:	Paper
Date Submitted by the Author:	07-Feb-2023
Complete List of Authors:	Xu, Heng; Duke University, Chemistry Chen, Zihao; Pennsylvania State University, Chemical Engineering Hao, Spencer; Duke University Fichthorn, Kristen; Pennsylvania State University, Chemical Engineering Wiley, Benjamin; Duke University, Chemistry

Chloride Enables the Growth of Ag Nanocubes and Nanowires by Making PVP Binding Facet-Selective

Heng Xu,†[a] Zihao Chen,†[b] Spencer Hao,[a] Kristen A. Fichthorn,*[b,c] and Benjamin J. Wiley*[a]

[a]Department of Chemistry, Duke University, Durham, NC 27708 (USA)

[b]Department of Chemical Engineering, Pennsylvania State University, University Park, PA 16802 (USA)

[c]Department of Physics, Pennsylvania State University, University Park, PA 16802 (USA)

† Equal Contributions by both authors.

*Benjamin J. Wiley (benjamin.wiley@duke.edu)

*Kristen A. Fichthorn (fichthorn@psu.edu)

Abstract

Solution-phase synthesis of metal nanocrystals with multiple additives is a common strategy for control over nanocrystal shape, and thus control over their properties. However, few rules are available to predict the effect of multiple capping agents on metal nanocrystal shapes, making it hard to rationally design synthetic conditions. This work uses a combination of seed-mediated growth, single-crystal electrochemistry, and DFT calculations to determine the roles of PVP and Cl^- in the anisotropic growth of single-crystal and penta-twinned silver nanocrystals. Single-crystal seeds grow into truncated octahedra bounded by a mixture of {111} and {100} facets in the presence of 0.03-30 mM PVP, but when 3~6 μM Cl^- is added with PVP, the single-crystal seeds grow into cubes bounded by {100} facets. Electrochemical measurements on Ag(100) and Ag(111) single-crystal electrodes show PVP is a capping agent but it exhibits no selectivity for a particular facet. Addition of Cl^- to PVP further passivates Ag(100) but not Ag(111), leading to conditions that favor formation of nanocubes. DFT calculations indicate the preferential binding of Cl^- to Ag(100) causes preferential binding of PVP to Ag(100). The combined results indicate the presence or absence of Cl^- modulates binding of PVP to (100) facets, leading to the formation of nanocubes with Cl^-, or truncated octahedra without it.

1. Introduction

Silver nanocrystals are promising materials for catalysis,[1-9] electronics,[10-14] sensing,[15-19] and biomedical applications.[20-23] For such applications, controlling the shape of silver nanocrystals enables control over their properties. With respect to catalysis, silver nanocubes, nanooctahedra, and nanowires exhibit different activities towards hydrogen evolution, carbon dioxide reduction, and ethylene epoxidation owing to the presentation of different crystal facets.[2, 5-7, 24, 25] In the case of electronics, networks of silver nanowires with higher aspect ratios exhibit lower sheet resistivity at the same transmittance.[10, 12, 13, 26, 27] In the realm of biomedical applications, silver nanoplates with high aspect ratios are used for photoacoustic imaging due to their high infrared absorption.[20] Therefore, developing and understanding synthetic methods to control the shapes of silver nanocrystals is essential to obtain desired functions.

For the colloidal synthesis of metal nanocrystals, one or multiple capping agents are usually added to control nanocrystal shape.[28, 29] It has been hypothesized that a capping agent can selectively adsorb on a specific crystal facet and block the deposition of metal atoms on that facet. As a result, metal deposition would slow on the capped facet and a specific shape would form based on the ratio (R) of growth rates along different crystallographic directions, e.g., along $\langle 100 \rangle$ and $\langle 111 \rangle$.[30-34]

Among various capping agents, polyvinylpyrrolidone (PVP) is widely used for the synthesis of silver nanocrystals. PVP is often considered as a {100} capping agent for silver because it is used in the production of silver nanocubes and nanowires bounded by{100} facets.[28] However, for the syntheses of silver nanowires with PVP, all reported syntheses also utilize Cl^- or Br^-.[10, 12, 13, 35, 36] Many syntheses of silver nanocubes with PVP also require the presence of Cl^- or Br^-.[37-42] The fact that these syntheses of nanowires and nanocubes require a halide indicates PVP by itself is not a strong capping agent of {100} facets. Some authors have proposed halides act as capping agents of {100} facets,[35, 40, 43] while others

propose halides cause nanocube formation by lowering the surface energy of {100} facets.[38] Other evidence contradicting PVP's potential role as a {100} capping agent is that it has been used alone or in conjunction with other additives for the syntheses of silver nanocrystals mainly covered by {111} facets, such as nanooctahedra, decahedra, icosahedra, and nanoplates.[2, 41, 44-47] A further complicating factor is that nanowires and nanoplates contain planar defects that likely promote anisotropic growth, making it difficult to quantify the contribution of PVP to these anisotropic shapes.[29, 48] Overall, both {100} and {111}-faceted silver nanocrystals can be synthesized with PVP as a capping agent, but the shape formed with PVP is usually co-determined with other species (i.e., Cl^- and Br^-) and defects. A lack of understanding of the roles of various additives and defects as well as the synergy between them makes it difficult to rationally design synthetic conditions for a specific shape.

To determine the processes causing anisotropic growth in various metal nanocrystal syntheses, we used single-crystal electrodes to measure facet-selective rates of atomic addition. We assume that the growth of the metal nanoparticle involves the reduction of metal ions by a reducing agent at a metal surface. By measuring how various additives affect the rate of metal ion reduction or reducing agent oxidation on Ag(100) or Ag(111) single-crystal electrodes, we can test hypotheses for how additives modulate atomic addition to different facets of nanocrystals that exhibit the same atomic packings. Changes in the rate of metal atom deposition to (111) and (100) single-crystal electrodes upon the addition of various additives were used to elucidate the facet-selective processes that cause anisotropic growth for the case of gold nanorods,[49] silver octahedra and nanoplates,[50] copper nanowires,[51, 52] and copper microplates.[53] For the case of copper nanowires and copper microplates, *ab initio* thermodynamics calculations based on density-functional theory (DFT) were used to provide insights into the structure of the adsorbate layer that caused anisotropic growth.[52, 54, 55] For example, for the case of copper nanowires, electrochemical measurements showed a narrow range of Cl^- concentrations selectively activated atomic

addition to Cu(111). Calculations showed that an intermediate monolayer coverage of Cl^- can selectively displace an alkylamine monolayer from {111} facets but not {100} facets, thereby enabling selective atomic addition to the {111} facets at the ends of a nanowire but not the {100} facets on the sides of a nanowire.[52, 54]

In this work, we combine synthesis, electrochemical measurements, and DFT calculations to investigate the roles of PVP and Cl^- in the anisotropic growth of silver nanocrystals. Synthetic results indicate PVP is a strong passivating agent with a slight preference for binding to (111) facets, which caused single-crystal silver seeds to grow into truncated octahedra and decahedral silver seeds grow into larger decahedra. However, single-crystal electrochemistry experiments show the addition of Cl^- with PVP selectively passivates {100} facets by 57.1%. This facet-selective effect is large enough to cause the growth of single-crystal seeds into nanocubes. The ratio of atomic addition to Ag(100) and Ag(111) single-crystal electrodes closely predicts the shape resulting from growth of single-crystal seeds. For penta-twinned seeds, the presence of twin defects causes 52 times more anisotropic growth than can be accounted for by passivation of the {100} facets on the sides of nanorods by Cl^-. *Ab initio* thermodynamic calculations indicate PVP binds similarly to Ag(100) and Ag(111), but when the Ag surfaces are partially covered by Cl^-, the PVP binding energy becomes stronger on Ag(100) than Ag(111), creating a range of PVP concentrations where PVP selectively binds Ag(100). The combined results indicate that nanocubes and nanowires form due to Cl^- adsorption to (100) facets, which in turn enhances the binding of PVP to (100) facets. For nanorods, the twin defects on the ends of the nanorods further catalyze atomic deposition to the end facets, leading to a much greater degree of anisotropy than can be explained by the facet-selective passivation of (100) facets by Cl^- and PVP.

2. Results and Discussion

2.1 Facet-Selective Growth of Single-Crystal Seeds with PVP and Cl^-

To understand how PVP and Cl^- determine the shape of single-crystal silver nanocrystals, we first investigated their roles in the growth of truncated silver nanocube seeds (**Figure 1A, B**). Since truncated cubes are single-crystal seeds enclosed by {100} and {111} facets, the growth of such seeds depends on how PVP and Cl^- interact with the {100} and {111} facets. The final shape that results from the growth of the single-crystal seeds is determined by the ratio (R) of growth rates along the ⟨100⟩ and ⟨111⟩ directions:

$$R = \frac{Growth_{<100>}}{Growth_{<111>}} \quad (1)$$

For single-crystal seeds, R can be estimated from the shape of the nanocrystals (**Figure S1**).[65] As the shape changes from a cube to an octahedron, R increases from 0.58 to 1.73.

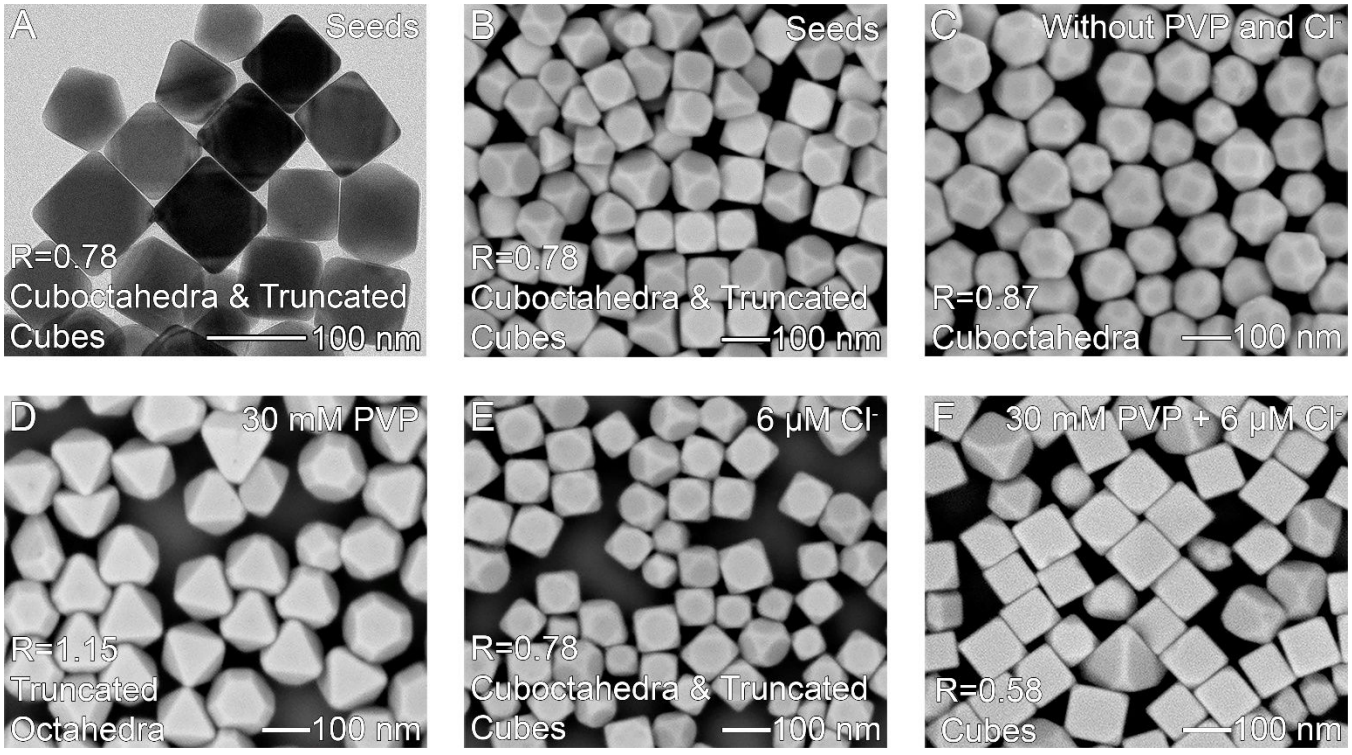

Figure 1. (A) TEM and (B) SEM images of the single-crystal seeds. (C-F) Results from growth of the single-crystal seeds with different amounts of PVP (MW=29,000) and Cl^-. (C) No PVP or Cl^-, (D) 30 mM PVP, (E) 6 μM Cl^-, and (F) 30 mM PVP and 6 μM Cl^-.

In the absence of PVP and Cl^-, the single-crystal seeds grew to form cuboctahedra, yielding an R of 0.87 (**Figure 1C**). With 30 mM PVP (MW=29,000) the single-crystal seeds mainly grew to form truncated octahedra with an R of 1.15 (**Figure 1D**). With 6 μM Cl^-, the single-crystal seeds mainly grew to form truncated cubes with an average R of 0.78 (**Figure 1E**). With 30 mM PVP (MW=29,000) and 6 μM Cl^-, the single-crystal seeds mainly grew to form cubes with an $R \leq 0.58$ (**Figure 1F**). Thus, the combination of PVP and Cl^- has a passivating effect on (100) facets that is greater than PVP or Cl^- separately.

The formation of truncated octahedra with 30 mM PVP (MW=29,000) indicates PVP (MW=29,000) is a weak {111} capping agent, contrary to the previous hypothesis that PVP is a {100} capping agent.[28, 48, 56-59] Since this result contradicts previous literature, we further examined the role of PVP of other molecular weights in the growth of silver nanocrystals (**Figure 2**). The single-crystal seeds mostly grew into truncated octahedra or cuboctahedra with 2-pyrrolidone or PVP of molecular weights from 10,000 to 1300,000 (**Figures 2**). The only exception is for PVP with MW=3,500, for which the single-crystal seeds grew into cubes (**Figure 2D**). We tested the amount of Cl^- contamination in 2-pyrrolidone and PVP of different MWs with a $Hg(SCN)_2$-Fe(III) based UV-Vis method to determine if the formation of nanocubes with MW=3,500 was due to Cl^- contamination.[60] **Figure S2** and Table S1 show all samples except PVP (MW=3,500) have sub-micromolar Cl^- contamination per 30 mM PVP. In contrast, a 2.5 M aqueous solution of PVP with MW=3,500 contained 0.7729 ± 0.0205 mM Cl^-, which leads to 9.2758 μM of Cl^- contamination in the synthesis with 30 mM PVP. This indicates the formation

of nanocubes in 30 mM PVP (MW=3,500) is likely due to Cl^- contamination rather than a different facet selectivity than PVP of other molecular weights.

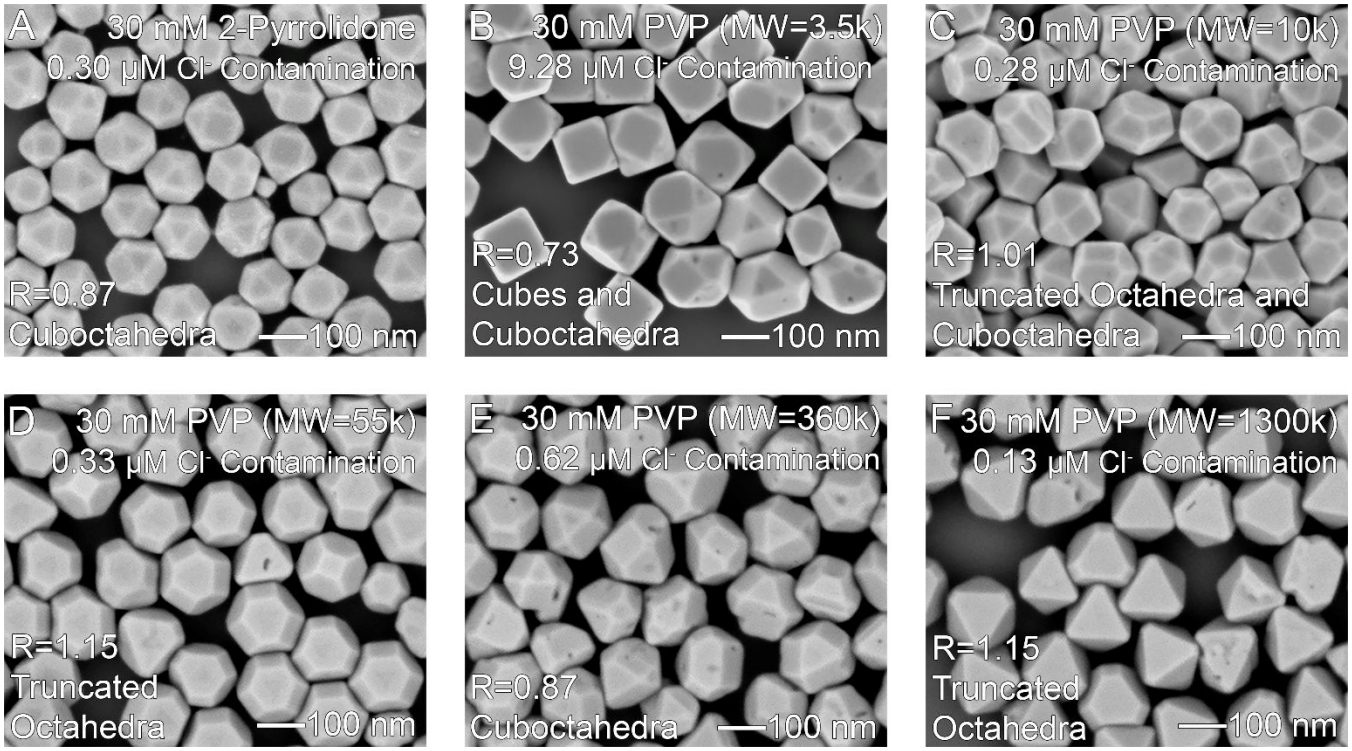

Figure 2. SEM images of the nanocrystals grown from the single-crystal seeds in the presence of 30 mM PVP with different MW's. (A) 2-Pyrrolidone, (B) MW=3,500, (C) MW=10,000, (D) MW=55,000, (E) MW=360,000, and (F) MW=1300,000. Note the formation of cubes in (B) was caused by contamination of the PVP with Cl^-.

2.2 Single-Crystal Electrochemical Measurements

We used single-crystal electrochemical measurements to quantify the effects of PVP (MW=29,000) and Cl^- on the silver deposition rate along ⟨100⟩ and ⟨111⟩.[50] The reaction for the seed-mediated growth

process is $2Ag^+ + AA \rightarrow 2Ag + DHA + 2H^+$. This reaction can be separated into two half-cell reactions, net Ag^+ reduction and AA oxidation. The full reaction happens at the mixed potential, which is the potential at which the cathodic and anodic current densities are equal and opposite to each other.[61] The current density at the mixed potential (j_{mp}) gives the rate of atomic deposition on the measured facet.

The linear sweep voltammograms (LSVs) obtained with the Ag(100) and Ag(111) electrodes for the Ag^+ reduction and AA oxidation half-reactions are shown in **Figure 3**. The resulting $R_j = j_{mp}^{(100)}/j_{mp}^{(111)}$ is compared to the synthetic results in **Table 1**. In the absence of PVP and Cl^- (**Figure 3A**), the j_{mp} on the Ag(100) electrode ($j_{mp}^{(100)}$) is 0.1050 mA/cm^2 and the j_{mp} on the Ag(111) electrode ($j_{mp}^{(111)}$) is 0.0897 mA/cm^2, giving R_j = 1.17. When 30 mM PVP is added (**Figure 3B**), $j_{mp}^{(100)}$ = 0.0310 mA/cm^2 and $j_{mp}^{(111)}$ = 0.0266 mA/cm^2, giving R_j =1.16. This R_j is very close to the R of 1.15 for truncated cubes formed with 30 mM PVP. Relative to the condition without PVP, the $j_{mp}^{(100)}$ decreased by 70.5% and the $j_{mp}^{(111)}$ decreased by 70.3 %. The similar R_j for the two facets and large decrease in current indicate PVP is a passivator but is not facet selective. Note, however, that the addition of PVP to the solution did not change the LSV for Ag^+ reduction for either electrode. All the decrease in the j_{mp} was due to the decrease in the current from AA oxidation. This indicates PVP is a strong passivator for the AA oxidation half-reaction but not for Ag^+ reduction.

With 6 μM Cl^- (see **Figure 3C**), $j_{mp}^{(100)}$ = 0.0758 mA/cm^2 and $j_{mp}^{(111)}$ = 0.1001 mA/cm^2, giving R_j = 0.757. This R_j is close to the R of 0.78 measured for the growth of single-crystal seeds with 6 μM Cl^-. The AA oxidation rate is suppressed by about 30% on Ag(100) with 6 μM Cl^- while Ag^+ reduction does not change. This indicates Cl^- weakly passivates AA oxidation but not Ag^+ reduction on {100} facets.

When 30 mM PVP and 6 μM Cl^- are added (**Figure 3D**), $j_{mp}^{(100)}$ = 0.0133 mA/cm^2 and $j_{mp}^{(111)}$ = 0.0297 mA/cm^2, giving R_j = 0.448. As with the other conditions, all the observed changes in j_{mp} are due

to the effects of the additives on the AA oxidation half-reaction. Relative to the condition with 30 mM PVP, we see the addition of 6 μM Cl^- decreased $j_{mp}^{(100)}$ by 57.1% and increased $j_{mp}^{(111)}$ by 11.6%. Thus, we observe that Cl^- passivates {100} and activates {111}, resulting in low enough values of R_j to favor the formation of cubes, thereby matching the synthetic results. The low value of R_j is mainly a result of the passivation of {100} by Cl^-, and the activation of {111} by Cl^- is relatively small.

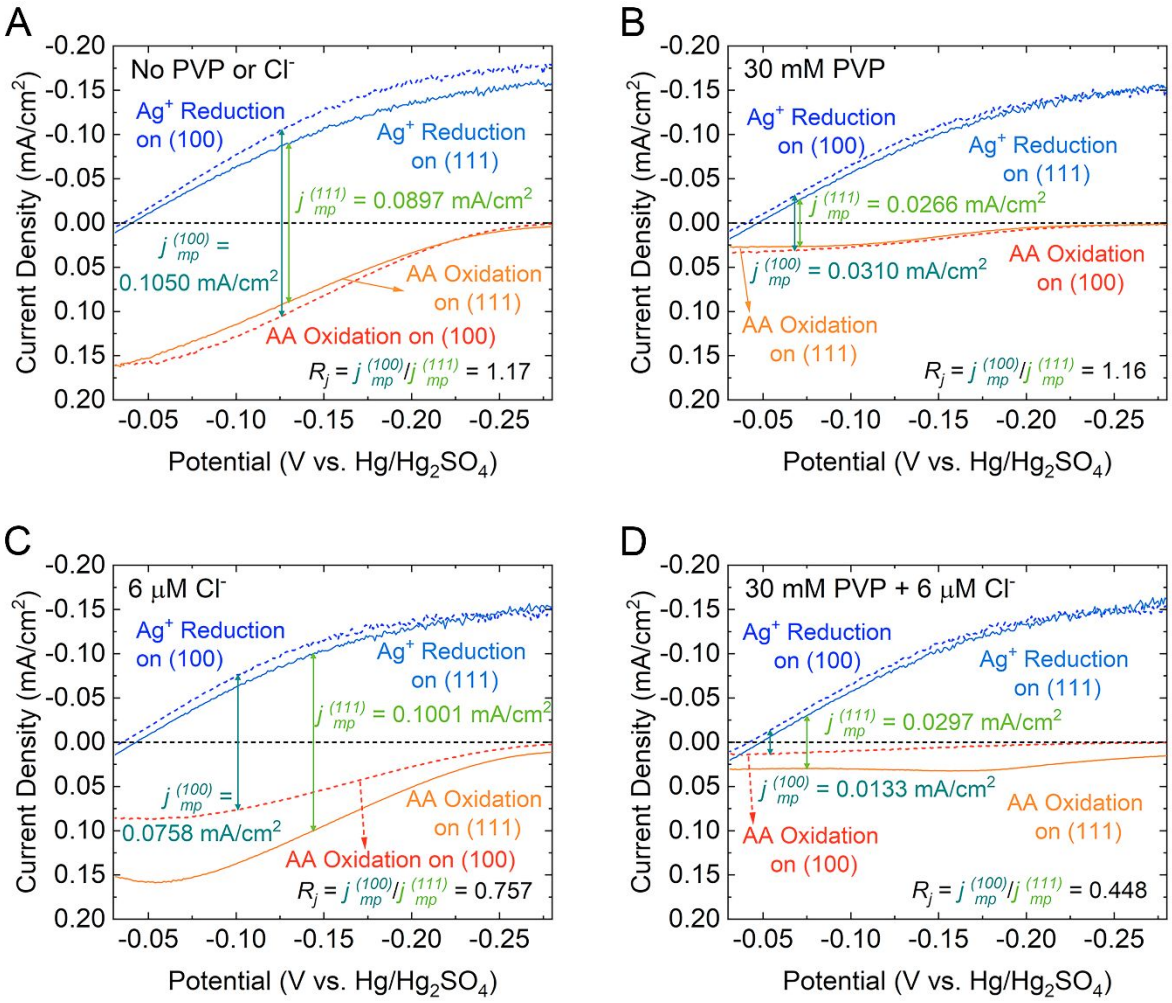

Figure 3. LSVs for Ag^+ reduction and AA oxidation half-reaction on Ag(100) and Ag(111) electrodes (A) without PVP and Cl^-, (B) with 30 mM PVP, (C) with 6 μM Cl^-, and (D) with 30 mM PVP and 6 μM Cl^-.

Table 1. Summary of R from analysis of the synthesized shape and R_j from electrochemical measurements for different experimental conditions. The shape from R_j is the shape that would have formed if the ratio

of the rates of atomic addition to the Ag(100) and Ag(111) single-crystal electrodes matched the ratio of atomic addition to {100} and {111} nanocrystal facets.

Synthetic Condition	R	Synthesized Shape	R_j	Shape from R_j	Effect of Additives
Without PVP or Cl^-	0.87	Cuboctahedra	1.17	Truncated Octahedra	N.A.
6 μM Cl^-	0.78	Truncated Cubes	0.757	Truncated Cubes	Cl^- Passivates {100}
30 mM PVP	1.15	Truncated Octahedra	1.16	Truncated Octahedra	PVP passivates {100} and {111}
30 mM PVP & 6 μM Cl^-	0.58	Cubes	0.448	Cubes	Cl^- and PVP passivates {100}

2.3 Effect of PVP and Chloride Concentration

A wider range of PVP (0.003-30 mM) and Cl^- (0.6 - 60 μM) concentrations were used to measure R for seed-mediated growth and to determine R_j with the single-crystal electrodes (**Table S2**). SEM images of the synthetic results and values for j_{mp}, R, and R_j are shown in **Figure S3, S4, S5** and **S6**. **Figure 4** summarizes the results with $j_{mp}^{(100)}$, $j_{mp}^{(111)}$, R and R_j plotted as a function of PVP and chloride concentration. **Figure 4A** shows PVP and Cl^- are passivators on Ag(100), and Ag(100) is the most passivated at high PVP and Cl^- concentrations. **Figure 4B** shows PVP is also a passivator on Ag(111), but Cl^- by itself does not have a strong effect on rates of atomic addition. Compared with Ag(100), Ag(111) is less passivated in the region of high PVP and Cl^- concentrations. **Figures 4C** and **4D** show plots of R_j and R as a function of Cl^- and PVP concentration. The two plots show a similar trend in the effects of PVP and Cl^- on the shape of Ag single crystals. With 10 ~ 30 mM PVP and no Cl^-, the single-crystal seeds grow into truncated octahedra. With 0.03 ~ 30 mM PVP and about 6 μM Cl^-, the single-crystal seeds grow into cubes. Under other intermediate conditions, the single-crystal seeds grow into intermediate shapes, such as truncated cubes and cuboctahedra. Interestingly, the concentration of Cl^- has a significant impact on the shape of Ag nanocrystals only when PVP is present but not when PVP is absent. A recent study on the polyol

synthesis of Ag nanocrystals with PVP has shown the shape of Ag nanocrystals is dependent on the concentration of Cl^-.[38] In this previous polyol study, the formation of Ag nanocubes was attributed to Cl^- lowering the surface energy of Ag(100). However, given that Ag nanocubes have never been synthesized in the presence of Cl^- without PVP or other capping agents, such as cetyltrimethylammonium (CTA^+), the effect of Cl^- on other capping agents may also play a vital role.[28, 43, 62, 63]

We note there are differences in the range of concentrations that cause nanocube vs. octahedra growth in the synthetic and electrochemical data; they are not completely identical. Some differences are expected due to the fact that, for example, the electrochemical experiments used the deposition rate at the initial reactant concentrations to represent the capping effect of PVP and Cl^-, but in the nanocrystal syntheses the concentrations of Ag^+ and AA continuously change. Other factors, such as edge effects, may also contribute to a difference in the shape of the synthesized nanocrystals from that predicted from the electrochemical experiments. Nevertheless, there is overall a strong similarity in the facet selective effects of PVP and Cl^- in both the synthetic and electrochemical experiments, indicating that the single-crystal electrodes provide a good model for the surface chemistry that occurs on the facets of the nanoparticles.

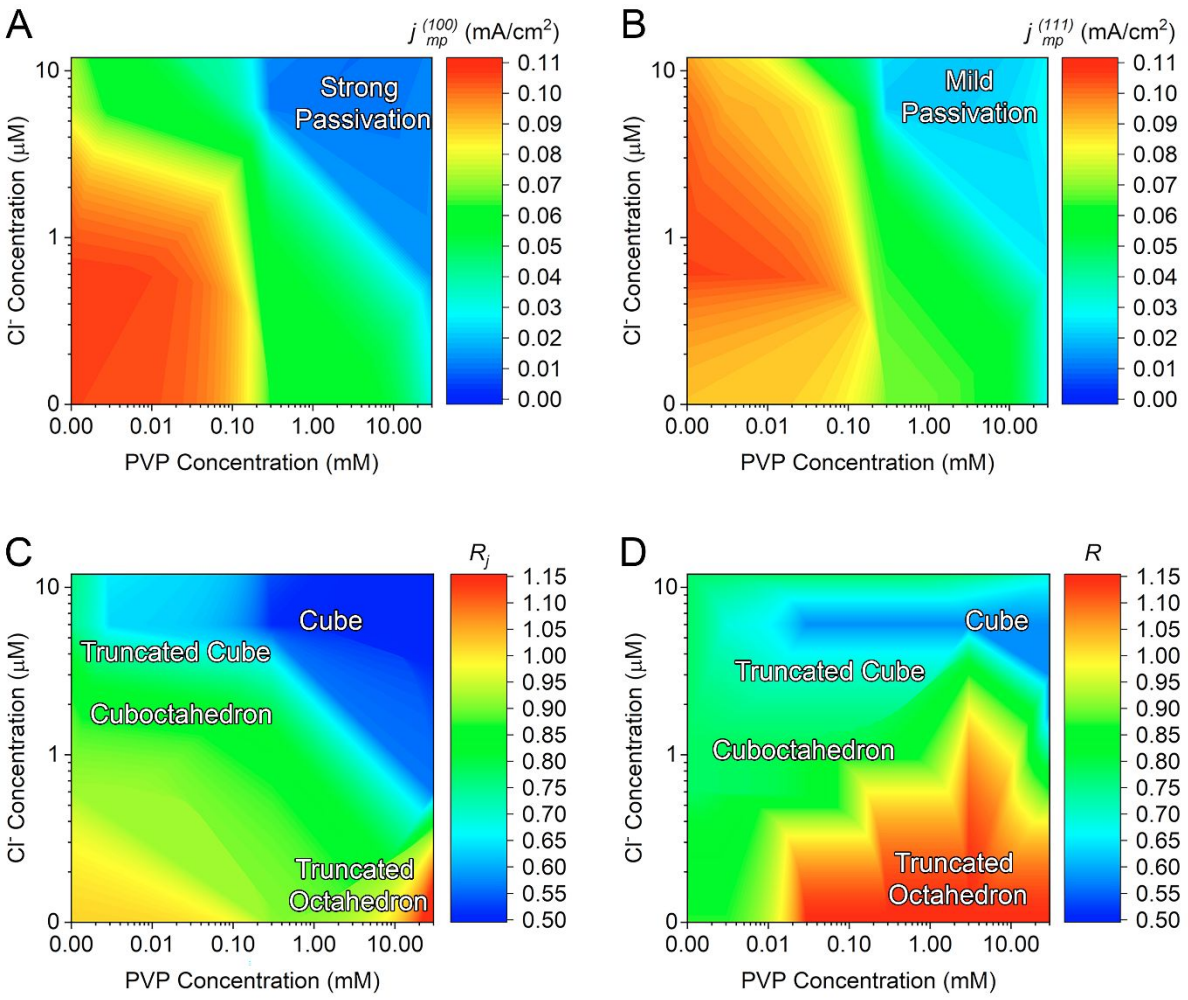

Figure 4. (A&B) Plots of Ag deposition rates on Ag(100) on Ag(111) single-crystal electrodes as a function of the concentration of PVP and Cl^-. (C) Plot of R_j, which predicts the nanocrystal shape based on electrochemical measurements of deposition rates, as a function of the concentration of PVP and Cl^-. (D) Plot of R, which quantifies the synthesized nanocrystal shape.

2.4 Effect of Planar Defects

Defects can also influence the anisotropic growth of silver nanocrystals. For example, for the seed-mediated growth of silver nanostructures with citrate, seeds with planar defects exhibit 30-100 times more anisotropic growth than single-crystal seeds under the same conditions.[50] The role of the planar defects was to act as a catalyst for atomic addition, while citrate prevented diffusion to {111} facets. Here, we use

silver decahedra with five-fold twin defects to measure the contribution of planar defects to the growth of silver nanorods in the presence of PVP and Cl^-. A model of a decahedron with labeled crystallographic directions is shown in **Figure S7**. [64] The silver decahedral seeds (**Figure 5A** and **5B**) are 43.8 ± 6.1 nm in width (*W*, measured) and 23.0 ± 3.2 nm in length (*L*, calculated). The decahedral seeds were synthesized by reduction of silver ions with citrate under blue light. For seed-mediated growth of silver decahedra, if the product shape is only determined by the rate of atomic addition to {100} and {111} facets, the decahedra would grow into larger decahedra when *R* is larger or equal to 1.73, and the decahedra would grow into rods when R is smaller than 1.73 (see **Figure S8** and the accompanying discussion in the Supporting Information).

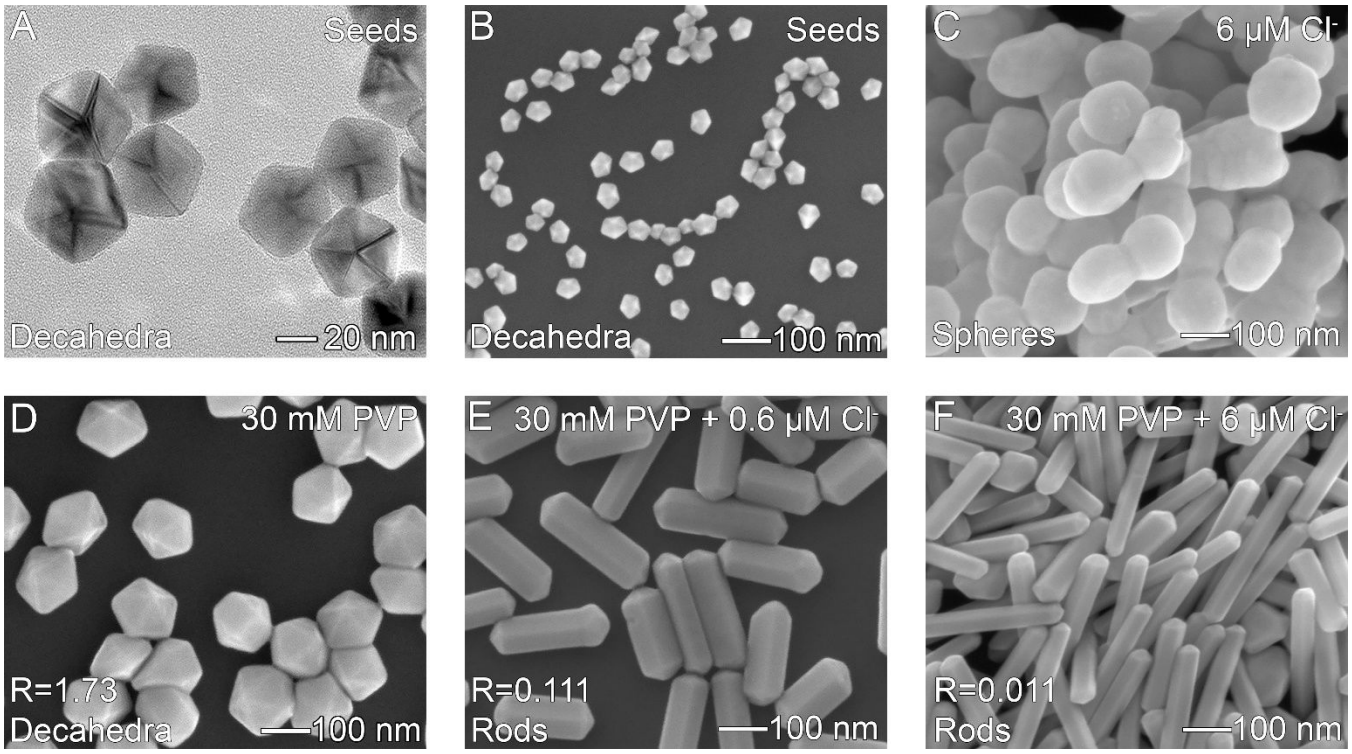

Figure 5. (A) TEM image and (B) SEM image of penta-twinned silver decahedron seeds. (C) The decahedral seeds grow into irregular spheres in the presence of 6 μM Cl^-. (D) The decahedral seeds grow into larger decahedra in the presence 30 mM PVP. (E) The decahedral seeds grow into short, thick rods

in the presence of 30 mM PVP and 0.6 μM Cl^-. (F) The decahedral seeds grow into long, thin rods in the presence of 30 mM PVP and 6 μM Cl^-.

With 6 μM Cl^- and no PVP, the silver decahedra grew into irregular spheres (**Figure 5C**). The same result is observed for all conditions without PVP (e.g., without PVP and without Cl^-, with 0.6 μM Cl^-, or with 60 μM Cl^-, see **Figure S9**). A possible reason is the twin planes in decahedra can catalyze silver atom deposition, similar to the planar defects in silver nanoplates,[50] and the presence of PVP is necessary to slow the deposition rate and allow decahedra to grow into well-defined shapes. In the presence of 30 mM PVP, the silver decahedra grew into larger decahedra, indicating R = 1.73 (**Figure 5D**). This result is similar to that obtained for the single-crystal seeds. When 30 mM PVP and 0.6 μM Cl^- are introduced, the silver decahedra grew into rods with $W = 74.2 \pm 10.4$ nm and $L = 213.4 \pm 34.0$ nm (**Figure 5E**). The average change in width (ΔW) is 30.4 nm and the average change in length (ΔL) is 190.4 nm, giving $R = 0.111$ ($R = 0.694\Delta W/\Delta L$). This value of R is 7.8 times smaller than the R value for single-crystal seeds grown under the same conditions. The procedure to calculate R from ΔW and ΔL can be found in the Supporting Information. When 30 mM PVP and 6 μM Cl^- are introduced, the silver decahedra grew into rods with $W = 48.7 \pm 4.8$ nm and $L = 331.1 \pm 70.4$ nm (**Figure 5F**). The average change in width (ΔW) is 4.9 nm and the average change in length (ΔL) is 308.0 nm, giving $R = 0.011$. This R is 52 times smaller than for single-crystal seeds grown under the same conditions. The fact that the increase in nanorod width is smaller than 5 nm agrees with the previously noted passivating effect of Cl^- on {100}.

The shape and much smaller value of R for the silver nanorods indicate the rate of atomic addition to the {111} surfaces of silver nanorods is up to 52 times greater than for single-crystal seeds. This result indicates the presence of twin defects catalyzes the deposition of silver atoms. However, there are five twin planes between the five {100} facets along the sides of silver rods as well as between the {111}

surfaces on the ends, but silver atom deposition is only increased to the {111} facets in the presence of PVP and Cl^-. With PVP alone, the decahedra grow into larger decahedra without facet-selective atomic deposition. The growth into decahedra may occur because both {111} and {100} surfaces are passivated by PVP. In contrast, the greater passivation of {100} surfaces in the presence of 30 mM PVP and 6 μM Cl^- led to preferential deposition of Ag on the ends of the nanorods.

2.5 DFT Calculations of PVP Adsorption

DFT calculations of PVP adsorption on Ag surfaces are challenging because PVP is a polymer. In this work, we represent PVP as divinylpyrrolidone (DVP), an isotactic dimer of PVP monomer (**Figure S10**). Moreover, these calculations do not include the solvent. In previous molecular-dynamics simulation studies of the Ag-PVP system, we found that while inclusion of solvent does weaken the PVP binding energy, the observed trends are the same as those from calculations without solvent.[65] To identify the optimal structure of DVP on Ag(100) and Ag(111), we probed various initial conformations at coverages of 0.063 and 0.11 monolayer (ML), where coverage is defined as the number of DVP per Ag surface atom. Details of the calculations are provided in the Supporting Information and the results of convergence tests are given in **Table S3**. We calculated the binding energy for each possible conformation using **Equation S9** and found four unique binding conformations on each Ag surface. The total binding energy can be partitioned into the energies of short-range, direct bonding interactions and van der Waals (vdW) interactions (**Table S4**). **Figure S11** depicts the optimal DVP conformations with the highest overall binding energies. Other possible DVP conformations are shown in **Figures S12** and **S13**.

The highest binding energy for DVP on Ag(100) is 1.13 eV and this quantity is 1.06 eV on Ag(111) (**Table S4**). The similar binding energies on the two facets imply PVP would bind to Ag(111) and Ag(100) to the same degree in syntheses, yielding similar growth rates along $\langle 100 \rangle$ and $\langle 111 \rangle$ ($R \approx 1$). This

interpretation agrees with the formation of truncated octahedra with 30 mM PVP (**Figure 1C**) and the electrochemical measurement that R_j = 1.16 (**Figure 3B**).

2.6 DFT calculations of the Effect of Chloride and PVP Co-Adsorption on Nanocrystal Morphology

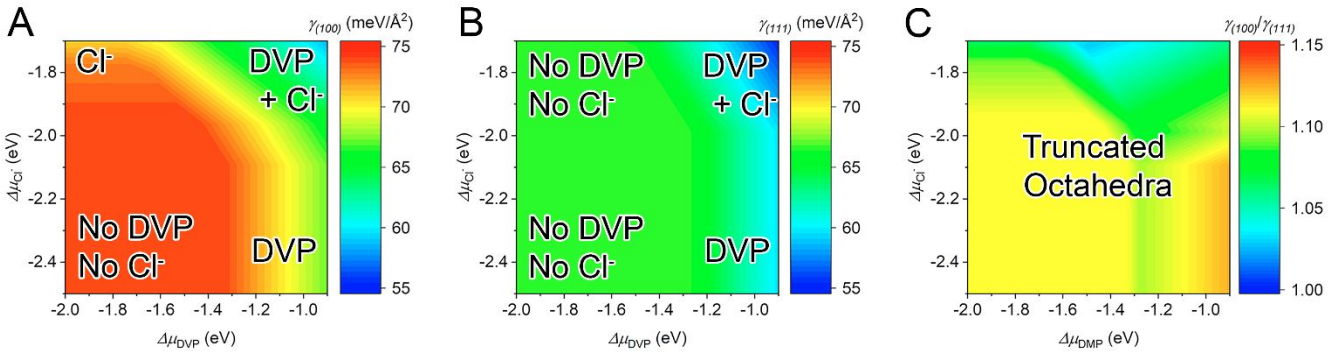

Figure 6. (A) $\gamma_{(100)}$ at different $\Delta\mu_{DVP}$ and $\Delta\mu_{Cl^-}$. (B) $\gamma_{(111)}$ at different $\Delta\mu_{DVP}$ and $\Delta\mu_{Cl^-}$. (C) $\gamma_{(100)}/\gamma_{(111)}$ at different $\Delta\mu_{DVP}$ and $\Delta\mu_{Cl^-}$.

To understand the effect of PVP and Cl^- co-adsorption on the growth of Ag nanocrystals, the DVP binding energy on Ag(100) and Ag(111) (**Figure S14**, **Table S5**), the surface energies of Ag(100) ($\gamma_{(100)}$) and Ag(111) ($\gamma_{(100)}$) (**Figure 6**), and the surface coverages of DVP and Cl^- (**Figure 7, S15, Table S6**), were calculated across a range of DVP chemical potentials ($\Delta\mu_{DVP}$) and Cl^- chemical potentials ($\Delta\mu_{Cl^-}$) . The Cl^- and DVP chemical potentials are expressed as $\Delta\mu$ in **Figure 6** and **Figure 7**, where Δ is the difference between the solution-phase chemical potential and the DFT total energy of the species in vacuum. The chemical potential is proportional to the concentration, with lower values corresponding to lower concentrations.

The surface energy calculations show $\gamma_{(100)}$ is generally slightly higher than $\gamma_{(111)}$, yielding a ratio of $\gamma_{(100)}/\gamma_{(111)}$ slightly larger than 1.00 at most $\Delta\mu_{DVP}$ and $\Delta\mu_{Cl^-}$ (**Figure 6**). Based on the Wulff

construction, any $\gamma_{(100)}/\gamma_{(111)}$ ratio between 0.87 and 1.73 would lead to the formation of truncated octahedra as the most stable product if the growth is controlled by thermodynamics. The $\gamma_{(100)}/\gamma_{(111)}$ ratio of around 1.00 at high $\Delta\mu_{DVP}$ and $\Delta\mu_{Cl^-}$ is significantly higher than the ratio required for the formation of cubes (no larger than 0.58), which contradicts the fact that the single-crystal seeds grow into cubes in the presence of 30 mM PVP and 6 μM Cl^- (**Figure 1F**), and indicates the growth of nanocubes is not controlled by thermodynamics, in agreement with the conclusions of some previous studies.[32, 34, 66-68] We further tested the possibility of forming truncated octahedra in the presence of PVP through surface diffusion by stirring single-crystal seeds in the presence of PVP (**Figure S16**). The seeds maintained the same shape under the same seed-mediated growth condition (**Figure S16A**), and no shape changes occurred to the seeds even at a longer reaction time and a higher temperature (**Figure S16B, C**). This indicates the shape of Ag nanocrystals is largely locked after silver atom deposition, and shape transformation to a thermodynamically more stable shape via surface diffusion is not possible under our experimental conditions.

To illustrate the extent to which Cl^- and DVP binding is facet-selective, **Figure 7** shows the surface coverages of Cl^- and DVP as a function of $\Delta\mu_{DVP}$ and $\Delta\mu_{Cl^-}$. A surface coverage level is defined as the percentage of coverage ($C\%$) of a species relative to its maximum surface coverage ($Cl^-\ C\% = Cl^-$ Coverage/0.50, $DVP\ C\% = DVP$ Coverage/0.11).

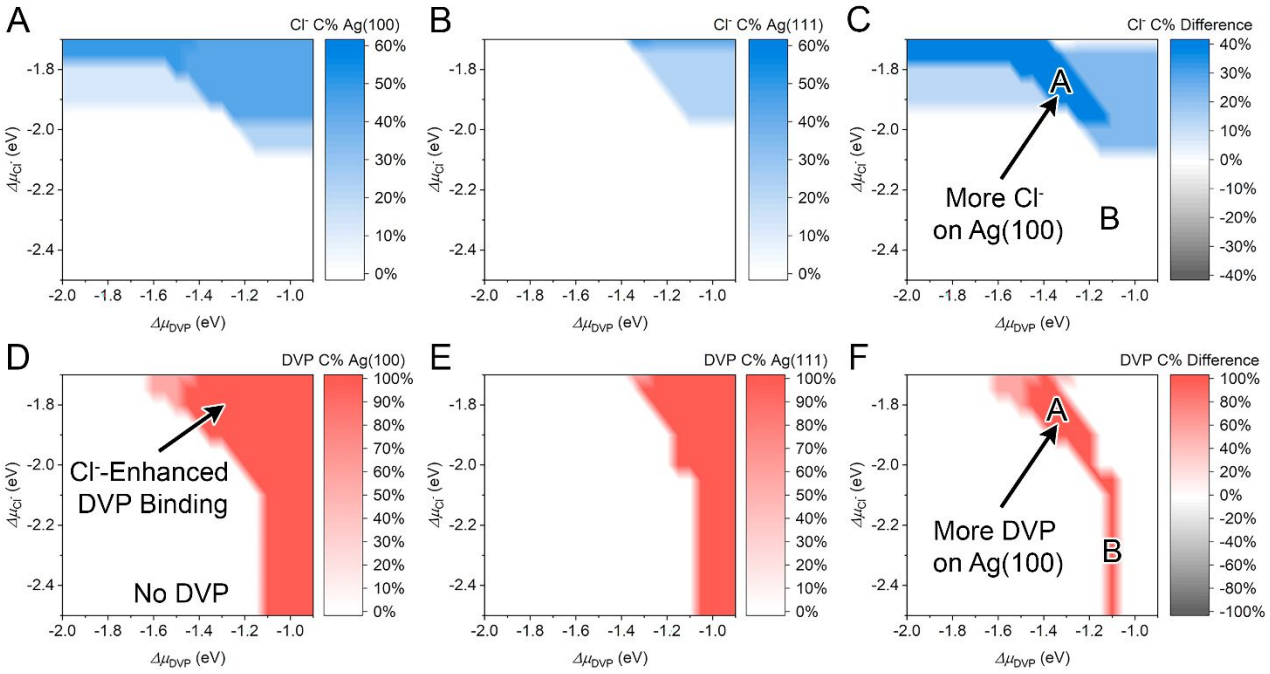

Figure 7. (A) Cl^- $C\%$ on Ag(100). (B) Cl^- $C\%$ on Ag(111). (C) Cl^- $C\%$ difference (Cl^- $C\%_{(100)} - Cl^-$ $C\%_{(111)}$) between Ag(100) and Ag(111). A higher $C\%$ indicates greater coverage on Ag(100). (D) DVP $C\%$ on Ag(100). (E) DVP $C\%$ on Ag(111). (F) DVP $C\%$ difference (DVP $C\%_{(100)} - DVP$ $C\%_{(111)}$) between Ag(100) and Ag(111). A higher $C\%$ indicates greater coverage on Ag(100).

As shown in **Figure 7A** and **7B**, the binding of Cl⁻ to Ag(100) occurs at a $\Delta\mu_{Cl^-}$ as low as -1.9 eV, while the binding of Cl⁻ to Ag(111) does not occur even when $\Delta\mu_{Cl^-} = -1.7\ eV$. In addition, the Cl⁻ coverage is generally higher on Ag(100) than Ag(111) (**Figure 7A, B**). A color map of the Cl^- $C\%$ difference between Ag(100) and Ag(111) (Cl^- $C\%_{(100)} - Cl^-$ $C\%_{(111)}$) illustrates the coverage of Cl⁻ on Ag(100) is nearly always greater than on Ag(111) (**Figure 7C**).

Figures 7D and 7E show the surface coverage of DVP on Ag(100) and Ag(111). At low chemical potentials ($\Delta\mu_{DVP} < -1.7\ eV$), DVP is always absent from both surfaces. At high chemical potentials ($\Delta\mu_{DVP} > -1.1\ eV$), DVP is always adsorbed to both surfaces. However, at an intermediate range of

chemical potentials ($-1.7\ eV \leq \Delta\mu_{DVP} \leq -1.1\ eV$), the value of $\Delta\mu_{Cl^-}$ modulates whether DVP is present or absent on Ag(100) and Ag(111) to a different extent. For example, at $\Delta\mu_{DVP} = -1.3\ eV$, the binding of DVP to Ag surfaces can occur at $-1.9\ eV \leq \Delta\mu_{Cl^-} \leq -1.7\ eV$, but DVP binding does not occur at $\Delta\mu_{Cl^-} < -1.9\ eV$. This indicates Cl^- adsorption can facilitate the binding of DVP. Binding energy calculations show the binding of DVP at higher $\Delta\mu_{Cl^-}$ is facilitated by a medium coverage (~50%, 0.25 ML) of Cl^-, which increases the binding energy of DVP by about 50% (**Figure S14**).

A color map of the DVP $C\%$ difference between Ag(100) and Ag(111) ($DVP\ C\%_{(100)} - DVP\ C\%_{(111)}$) shows two regions (regions A and B) where DVP exhibits facet-selective binding (**Figure 7F**). In region A, both DVP and Cl^- preferentially bind Ag(100) (**Figure 7C, F**). Note that below region A, a lower $\Delta\mu_{Cl^-}$ where no Cl^- adsorption occurs (**Figure 7A, B**), DVP does not adsorb on Ag(100) or Ag(111) (**Figure 7D, E**). This indicates in region A, the facet-selective binding of Cl^- on Ag(100) induces the facet-selective binding of DVP on Ag(100). We believe this chemical potential region corresponds to the synthetic conditions for nanocube growth in the presence of 0.03-30 mM PVP and about 6 μM Cl^- (**Figure 1F**, **S5F-H**).

There are two regions around region A where Cl^- exhibits facet-selective binding while DVP does not. To the left of region A, $\Delta\mu_{DVP}$ is too low for DVP to adsorb on either Ag facet (**Figure 7D, E**) even though Cl^- shows a binding preference for Ag(100) (**Figure 7A-C**). Without DVP, the facet-selective passivation of Cl^- on Ag(100) alone is not sufficient for the growth of cubes, but instead leads to the growth of truncated cubes in the presence of 6 μM Cl^- (**Figure 1E**). To the right of region A, a high $\Delta\mu_{DVP}$ leads to 100% coverage of DVP on both facets. In this case, the facet-selective binding of Cl^- to Ag(100) in conjunction with DVP binding may create a condition that is suitable for the growth of cubes.

In region B, DVP adsorbs on Ag(100) but not Ag(111) in the absence of Cl^- on either facet (**Figure 7D, E**). Although this calculation indicates there is a small range of DVP concentrations over which there is facet-selective binding of DVP on Ag(100) without Cl^-, the synthesis produced only truncated octahedra in the absence of Cl^- with PVP concentrations of 0.003-30 mM (**Figure 1D, Figure S5A-D**). If PVP were adsorbed specifically on {100} facets, the electrochemical data in **Figure 3A&B** indicate that PVP is a sufficiently good passivator that facet-selective adsorption on {100} facets would lead to the formation of nanocubes. It is possible that the PVP concentrations that we tested do not fall within the narrow range of region B. It is also possible that the simplifications used to make the calculations tractable, e.g., the use of DVP instead of PVP and the use of vacuum instead of water as a solvent, result in this mismatch between the calculated result and experiment. To the right of region B, DVP coverages on Ag(100) and Ag(111) are the same, which is likely to lead to an R that is close to 1.00, and therefore agrees with the growth of truncated octahedra in the presence of medium to high concentrations of PVP observed in experiments (**Figure 1D, S5B-D**).

3. Conclusions

In this study, we used nanocrystal synthesis, electrochemical measurements, and DFT calculations to investigate the roles of PVP and Cl^- in the growth of single-crystal and penta-twinned silver nanocrystals. PVP was found to have a similar strong passivating effect on (100) and (111) facets, leading to an electrochemically measured R_j = 1.16 (deposition rate on Ag(100)/Ag(111)), and the growth of single-crystal seeds into truncated octahedra with R = 1.15. DFT calculations show the binding of DVP to the two facets was also similar: 1.13 eV on Ag(100) and 1.06 eV on Ag(111). Addition of Cl^- with PVP enhanced passivation of (100) facets by 57%, leading to an electrochemically measured R_j = 0.58 and the growth of single-crystal seeds into nanocubes with R = 0.448. DFT calculations suggest this occurred due

to preferential binding of Cl^- to (100) facets, which in turn preferentially enhanced binding of DVP to (100) facets. Thus, we find a new mechanism for the anisotropic growth of silver nanocrystals in which facet-selective binding of a halide, Cl^-, to (100) facets caused preferential binding of a capping agent, PVP, to those same facets.

We further quantified the role of twin-defects in driving anisotropic growth by studying the seed-mediated growth of penta-twinned silver decahedra. Synthetic results show decahedra seeds grow into larger decahedra with PVP alone. When Cl^- is added with PVP, those same decahedra grow anisotropically to form nanorods. The anisotropic growth of nanorods is 52 times greater than that observed for single-crystal seeds under the same conditions, indicating the presence of twin defects are a powerful catalyst for atomic addition. Taken together, we hope this work helps to clarify the contributions of capping agents and defects in causing the anisotropic growth of silver nanostructures.

ASSOCIATED CONTENT

Supporting Information Available: Experimental and theoretical methods, schematic representations and dimensional measurements of different types of nanocrystals, additional LSV measurements, UV-Vis Spectra to determine the amount of Cl^- contamination, additional SEM images of the silver nanocrystals, DVP binding conformations, and DVP binding energies at different Cl^- coverages.

AUTHOR INFORMATION

Corresponding Authors

Kristen A. Fichthorn - Department of Chemical Engineering, The Pennsylvania State University, University Park, Pennsylvania 16802, United States;

*Email: fichthorn@psu.edu

ORCID: 0000-0002-4256-714X

Benjamin J. Wiley - Department of Chemistry, Duke University, Durham, North Carolina 27708, United States;

*E-mail: benjamin.wiley@duke.edu

ORCID: 0000-0002-1314-6223

Authors

Heng Xu - Department of Chemistry, Duke University, Durham, North Carolina 27708, United States

Email: heng.xu@duke.edu

ORCID: 0000-0002-8259-5516

Zihao Chen - Department of Chemical Engineering, Pennsylvania State University, University Park, PA 16802 (USA)

Email: zihaoc23@gmail.com

ORCID: 0000-0002-6733-4756

Spencer Hao - Duke University, Durham, North Carolina 27708, United States

Email: spencer.hao@duke.edu

ORCID: 0000-0003-4463-0138

Author Contributions

Heng Xu and Zihao Chen contributed equally to this manuscript.

Conflicts of Interest

There are no conflicts to declare.

ACKNOWLEDGMENT

This work was supported by NSF Grant No. CHE-1808108 (H.X., S.H., and B.J.W.) and by the Department of Energy, Office of Basic Energy Sciences, Materials Science Division, DE-FG02-07ER46414 (Z.C. and K.A.F.). Z.C. acknowledges training provided by the Computational Materials Education and Training (CoMET) NSF Research Traineeship (DGE-1449785). SEM and TEM were performed at the Duke University Shared Materials Instrumentation Facility (SMIF), a member of the North Carolina Research Triangle Nanotechnology Network (RTNN), which is supported by the National Science Foundation (award number ECCS-2025064) as part of the National Nanotechnology Coordinated Infrastructure (NNCI).

References

1. S. Liu, H. Tao, L. Zeng, Q. Liu, Z. Xu, Q. Liu and J.-L. Luo, *J. Am. Chem. Soc.*, 2017, **139**, 2160-2163.
2. T.-R. Kuo, Y.-C. Lee, H.-L. Chou, S. M G, C.-Y. Wei, C.-Y. Wen, Y.-H. Chang, X.-Y. Pan and D.-Y. Wang, *Chem. Mater.*, 2019, **31**, 3722-3728.
3. Z. Li, J.-Y. Fu, Y. Feng, C.-K. Dong, H. Liu and X.-W. Du, *Nat. Catal.*, 2019, **2**, 1107-1114.
4. M. de Jesus Gálvez-Vázquez, P. Moreno-García, H. Xu, Y. Hou, H. Hu, I. Z. Montiel, A. V. Rudnev, S. Alinejad, V. Grozovski, B. J. Wiley, M. Arenz and P. Broekmann, *ACS Catal.*, 2020, **10**, 13096-13108.
5. P. Christopher and S. Linic, *J. Am. Chem. Soc.*, 2008, **130**, 11264-11265.
6. P. Christopher and S. Linic, *ChemCatChem*, 2010, **2**, 78-83.
7. K. B. Zhou and Y. D. Li, *Angew. Chem. Int. Ed.*, 2012, **51**, 602-613.
8. Y. Shi, Z. Lyu, M. Zhao, R. Chen, Q. N. Nguyen and Y. Xia, *Chem. Rev.*, 2021, **121**, 649-735.
9. M. J. Landry, A. Gellé, B. Y. Meng, C. J. Barrett and A. Moores, *ACS Catal.*, 2017, **7**, 6128-6133.
10. S. M. Bergin, Y.-H. Chen, A. R. Rathmell, P. Charbonneau, Z.-Y. Li and B. J. Wiley, *Nanoscale*, 2012, **4**, 1996-2004.
11. G. Khanarian, J. Joo, X.-Q. Liu, P. Eastman, D. Werner, K. O'Connell and P. Trefonas, *J. Appl. Phys.*, 2013, **114**, 024302.
12. B. Li, S. Ye, I. E. Stewart, S. Alvarez and B. J. Wiley, *Nano Lett.*, 2015, **15**, 6722-6726.
13. Z. Niu, F. Cui, E. Kuttner, C. Xie, H. Chen, Y. Sun, A. Dehestani, K. Schierle-Arndt and P. Yang, *Nano Lett.*, 2018, **18**, 5329-5334.
14. T. Sannicolo, M. Lagrange, A. Cabos, C. Celle, J. P. Simonato and D. Bellet, *Small*, 2016, **12**, 6052-6075.
15. C. Gao , Z. Lu , Y. Liu , Q. Zhang, M. Chi, Q. Cheng and Y. Yin, *Angew. Chem. Int. Ed.*, 2012, **51**, 5629-5633.

16. Q. Zhang, C. H. Moran, X. Xia, M. Rycenga, N. Li and Y. Xia, *Langmuir*, 2012, **28**, 9047-9054.
17. K.-S. Lee and M. A. El-Sayed, *J. Phys. Chem. B*, 2006, **110**, 19220-19225.
18. X. Li, C. Batchelor-McAuley and R. G. Compton, *ACS Sens.*, 2019, **4**, 464-470.
19. M. Banchelli, B. Tiribilli, M. de Angelis, R. Pini, G. Caminati and P. Matteini, *ACS Appl. Mater. Interfaces*, 2016, **8**, 2628-2634.
20. K. A. Homan, M. Souza, R. Truby, G. P. Luke, C. Green, E. Vreeland and S. Emelianov, *ACS Nano*, 2012, **6**, 641-650.
21. L. M. Stabryla, K. A. Johnston, N. A. Diemler, V. S. Cooper, J. E. Millstone, S.-J. Haig and L. M. Gilbertson, *Nat. Nanotechnol.*, 2021, DOI: 10.1038/s41565-021-00929-w.
22. E. C. Dreaden and M. A. El-Sayed, *Acc. Chem. Res.*, 2012, **45**, 1854-1865.
23. N. Macia, R. Bresoli-Obach, S. Nonell and B. Heyne, *J. Am. Chem. Soc.*, 2019, **141**, 684-692.
24. S. Xie, S.-I. Choi, X. Xia and Y. Xia, *Curr. Opin. Chem. Eng.*, 2013, **2**, 142-150.
25. S. Liu, C. Sun, J. Xiao and J.-L. Luo, *ACS Catal.*, 2020, **10**, 3158-3163.
26. R. M. Mutiso, M. C. Sherrott, A. R. Rathmell, B. J. Wiley and K. I. Winey, *ACS Nano*, 2013, **7**, 7654-7663.
27. S. Ye, A. R. Rathmell, Z. Chen, I. E. Stewart and B. J. Wiley, *Adv. Mater.*, 2014, **26**, 6670-6687.
28. T.-H. Yang, Y. Shi, A. Janssen and Y. Xia, *Angew. Chem. Int. Ed.*, 2020, **59**, 15378-15401.
29. B. Wiley, Y. Sun, B. Mayers and Y. Xia, *Chem. Eur. J.*, 2005, **11**, 454-463.
30. Z. L. Wang, *J. Phys. Chem. B*, 2000, **104**, 1153-1175.
31. Y. Xiong and Y. Xia, *Adv. Mater.*, 2007, **19**, 3385-3391.
32. Z. Chen, J. W. Chang, C. Balasanthiran, S. T. Milner and R. M. Rioux, *J. Am. Chem. Soc.*, 2019, **141**, 4328-4337.
33. Y. W. Wang, J. T. He, C. C. Liu, W. H. Chong and H. Y. Chen, *Angew. Chem. Int. Ed.*, 2015, **54**, 2022-2051.
34. X. Qi, T. Balankura, Y. Zhou and K. A. Fichthorn, *Nano Lett.*, 2015, **15**, 7711-7717.
35. R. R. da Silva, M. Yang, S.-I. Choi, M. Chi, M. Luo, C. Zhang, Z.-Y. Li, P. H. C. Camargo, S. J. L. Ribeiro and Y. Xia, *ACS Nano*, 2016, **10**, 7892-7900.
36. B. Wiley, Y. Sun and Y. Xia, *Langmuir*, 2005, **21**, 8077-8080.
37. B. Wiley, T. Herricks, Y. Sun and Y. Xia, *Nano Lett.*, 2004, **4**, 1733-1739.
38. Z. Chen, T. Balankura, K. A. Fichthorn and R. M. Rioux, *ACS Nano*, 2019, **13**, 1849-1860.
39. S. H. Im, Y. T. Lee, B. Wiley and Y. Xia, *Angew. Chem. Int. Ed.*, 2005, **44**, 2154-2157.
40. A. Ruditskiy and Y. Xia, *J. Am. Chem. Soc.*, 2016, **138**, 3161-3167.
41. A. Tao, P. Sinsermsuksakul and P. Yang, *Angew. Chem. Int. Ed.*, 2006, **45**, 4597-4601.
42. K. M. Koczkur, S. Mourdikoudis, L. Polavarapu and S. E. Skrabalak, *Dalton Trans.*, 2015, **44**, 17883-17905.
43. S. Zhou, J. Li, K. D. Gilroy, J. Tao, C. Zhu, X. Yang, X. Sun and Y. Xia, *ACS Nano*, 2016, **10**, 9861-9870.
44. M. Tsuji, M. Ogino, R. Matsuo, H. Kumagae, S. Hikino, T. Kim and S.-H. Yoon, *Cryst. Growth Des*, 2010, **10**, 296-301.
45. Y. Gao, P. Jiang, L. Song, J. X. Wang, L. F. Liu, D. F. Liu, Y. J. Xiang, Z. X. Zhang, X. W. Zhao, X. Y. Dou, S. D. Luo, W. Y. Zhou and S. S. Xie, *J. Cryst. Growth*, 2006, **289**, 376-380.
46. I. Washio, Y. Xiong, Y. Yin and Y. Xia, *Adv. Mater.*, 2006, **18**, 1745-1749.
47. Q. Zhang, N. Li, J. Goebl, Z. Lu and Y. Yin, *J. Am. Chem. Soc.*, 2011, **133**, 18931-18939.
48. Y. Sun, B. Mayers, T. Herricks and Y. Xia, *Nano Lett.*, 2003, **3**, 955-960.
49. M. Brown and B. J. Wiley, *Chem. Mater.*, 2020, **32**, 6410-6415.
50. H. Xu and B. J. Wiley, *Chem. Mater.*, 2021, **33**, 8301-8311.
51. M. J. Kim, P. F. Flowers, I. E. Stewart, S. Ye, S. Baek, J. J. Kim and B. J. Wiley, *J. Am. Chem. Soc.*, 2017, **139**, 277-284.
52. M. J. Kim, S. Alvarez, Z. Chen, K. A. Fichthorn and B. J. Wiley, *J. Am. Chem. Soc.*, 2018, **140**, 14740-14746.
53. M. J. Kim, M. A. Cruz, Z. Chen, H. Xu, M. Brown, K. A. Fichthorn and B. J. Wiley, *Chem. Mater.*, 2021, **33**, 881-891.
54. K. A. Fichthorn and Z. Chen, *J. Vac. Sci. Technol. A*, 2020, **38**, 023210.

55. M. J. Kim, M. A. Cruz, Z. Chen, H. Xu, M. Brown, K. A. Fichthorn and B. J. Wiley, *Chem. Mater.*, 2020, DOI: 10.1021/acs.chemmater.0c03596, 10.1021/acs.chemmater.1020c03596.
56. Y. G. Sun and Y. N. Xia, *Science*, 2002, **298**, 2176-2179.
57. J. Zeng, Y. Zheng, M. Rycenga, J. Tao, Z.-Y. Li, Q. Zhang, Y. Zhu and Y. Xia, *J. Am. Chem. Soc.*, 2010, **132**, 8552-8553.
58. X. Xia, J. Zeng, L. K. Oetjen, Q. Li and Y. Xia, *J. Am. Chem. Soc.*, 2012, **134**, 1793-1801.
59. J. Zeng, X. Xia, M. Rycenga, P. Henneghan, Q. Li and Y. Xia, *Angew. Chem. Int. Ed.*, 2011, **50**, 244-249.
60. D. M. Zall, D. Fisher and M. Q. Garner, *Analytical Chemistry*, 1956, **28**, 1665-1668.
61. M. J. Kim, M. Brown and B. J. Wiley, *Nanoscale*, 2019, **11**, 21709-21723.
62. R. Long, S. Zhou, B. J. Wiley and Y. Xiong, *Chem. Soc. Rev.*, 2014, **43**, 6288-6310.
63. B. Wiley, Y. Sun and Y. Xia, *Acc. Chem. Res.*, 2007, **40**, 1067-1076.
64. Y. Xia, Y. Xiong, B. Lim and S. E. Skrabalak, *Angew. Chem. Int. Ed.*, 2009, **48**, 60-103.
65. T. Balankura, X. Qi and K. A. Fichthorn, *J. Phys. Chem. C*, 2018, **122**, 14566-14573.
66. X. Qi and K. A. Fichthorn, *Nanoscale*, 2017, **9**, 15635-15642.
67. X. Qi, T. Balankura and K. A. Fichthorn, *J. Phys. Chem. C*, 2018, **122**, 18785-18794.
68. K. A. Fichthorn, Z. Chen, Z. Chen, R. M. Rioux, M. J. Kim and B. J. Wiley, *Langmuir*, 2021, **37**, 4419-4431.